Tunable Casimir equilibria with phase change materials: From quantum trapping to its release

Lixin Ge,[1,*] Xi Shi,[2] Zijun Xu,[1] and Ke Gong[1]
[1]*School of Physics and Electronic Engineering, Xinyang Normal University, Xinyang 464000, China*
[2]*Department of Physics, Shanghai Normal University, Shanghai 200234, China*

(Received 23 October 2019; revised manuscript received 9 March 2020; accepted 10 March 2020; published 31 March 2020)

A stable suspension of nanoscale particles due to the Casimir force is of great interest for many applications such as sensing, noncontract nanomachines. However, the suspension properties are difficult to change once the devices are fabricated. Vanadium dioxide (VO_2) is a phase change material, which undergoes a transition from a low-temperature insulating phase to a high-temperature metallic phase around a temperature of 340 K. In this work, we study Casimir forces between a nanoplate (gold or Teflon) and a layered structure containing a VO_2 film. It is found that stable Casimir suspensions of nanoplates can be realized in a liquid environment, and the equilibrium distances are determined, not only by the layer thicknesses but also by the matter phases of VO_2. Under proper designs, a switch from quantum trapping of the gold nanoplate ("on" state) to its release ("off" state) as a result of the metal-to-insulator transition of VO_2, is revealed. On the other hand, the quantum trapping and release of a Teflon nanoplate is found under the insulator-to-metal transition of VO_2 . Our findings offer the possibility of designing switchable devices for applications in micro and nanoelectromechanical systems.

DOI: 10.1103/PhysRevB.101.104107

I. INTRODUCTION

Micro and nanoelectromechanical systems (MEMS and NEMS), which integrate electrical and mechanical functionality on the micro and nanoscales, have attracted enormous attention [1,2]. Thanks to small sizes, the MEMS and NEMS exhibit low mass, high mechanical resonance frequencies, and quantum effects, leading to a broad range of applications such as biological/chemical detections [3], accelerometers [4], and micro/nanomachines [5]. One major problem in MEMS and NEMS is the *stiction* which makes the systems collapse and permanent adhesion caused by the attractive Casimir forces [6,7]. The Casimir force is a macroscopic quantum effect which arises from quantum fluctuations of the electromagnetic field [8]. In most cases, two neutral, parallel plates consisted of the same materials are attractive to each other, and the magnitudes of the attraction depend on several parameters such as separations, geometric thicknesses, finite conductivities, and temperatures (see, e.g., the review [9] and Refs. [10,11]. Therefore, repulsive Casimir forces are highly required for noncontact and low-friction MEMS and NEMS. The repulsive Casimir forces have been intensively studied in many systems [12] including liquid-separated environments [13–16], metamaterials [17–20], topological insulators [21–23], two-dimensional materials [24–26], and specific geometrics [27,28]. In addition, the concept of Casimir equilibria was also investigated, using the enclosed geometries [29,30] and dispersive materials [31]. Lately, stable Casimir equilibria of nanoplates above a Teflon-coated gold substrate were reported by Zhao *et al.* [32]. However, the Casimir equilibria of previous studies were mainly in passive systems. Once the devices are fabricated, the trapping properties are difficult to change. Thus the tunable trapping or even the switching from the trapping to its release by external stimuli (e.g., heating, electric fields or optical waves) is highly desired in MEMS and NEMS.

To active modulate the Casimir effect, one straight way is to change the dielectric properties of materials under external means [33–38]. Vanadium dioxide (VO_2) [39,40] is a phase change material (PCM), which undergoes a transition from a low-temperature insulating phase to a high-temperature metallic phase at critical temperature 340 K. The phase transition of VO_2 is accompanied by a structural transformation from the monoclinic phase to the tetragonal one. Meanwhile, the dielectric function of VO_2 changes dramatically during the phase transition, leading to many interesting applications [41–44]. In general, the phase transition of VO_2 can be induced by changing the temperature of systems. Alternatively, the phase transition can be driven by optical lasers [45,46] or electrical gratings [47,48] on a subpicosecond timescale. Recently, VO_2 has been employed to study the tunable Casimir effect in the vacuum [49–51]. For a large separation (e.g., $> 1\ \mu$m), the contrast of Casimir forces due to the phase-transition is quite large (e.g., over two times for two semi-infinite plates of VO_2, this value could be even larger for the case of finite thickness [49,50]). As the separation is small (e.g., $\sim$100 nm), however, the modulation of Casimir forces owning to the phase transition and finite-thickness decreases greatly [50,51]. Nonetheless, the Casimir forces are always attractive and only magnitude modulations have been reported in a vacuum-separated configuration. The influences of phase transition of VO_2 on the sign modulation of Casimir forces (e.g., from attraction to repulsion) are yet less explored. In a liquid environment, the function of sign modulation and the related phenomenon such as tunable

*lixinge@hotmail.com

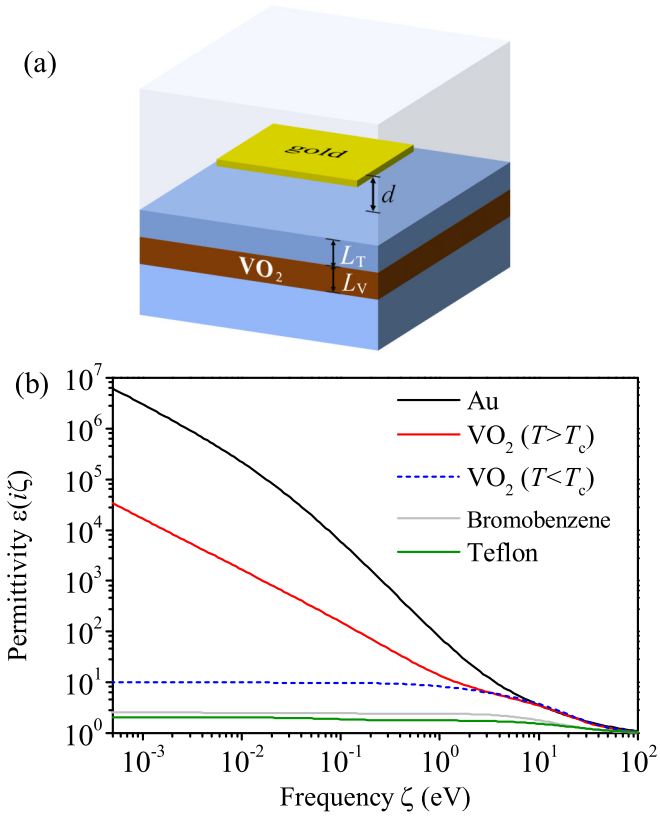

FIG. 1. (a) Schematic view of a gold nanoplate suspended in a liquid environment. (b) The permittivity of different materials (gold, VO_2, bromobenzene, and Teflon) as a function of imaginary frequency.

Casimir equilibria are expected based on the phase transition of VO_2.

Here the Casimir forces between a nanoplate and a layered structure separated by a liquid are investigated. The layered structure consists of two kinds of materials, i.e., Vanadium dioxide (VO_2) and Teflon. It is found that stable Casimir equilibria of gold nanoplates can be realized when a VO_2 film is buried under a semi-infinite Teflon. The properties of Casimir equilibria are determined, not only by the layer thicknesses but also by the matter phases of VO_2. For thick-film VO_2, the Casimir equilibria and quantum traps can be achieved for both the metallic and insulating phases. On the other hand, a switch from quantum trapping of the gold nanoplate ("on" state) to its release ("off" state) can be triggered by the metal-to-insulator phase transition when the thickness of VO_2 is thin (e.g., 20 nm). Finally, stable suspensions of Teflon nanoplates are also proposed with a complementary design, where the Teflon substrate is coated by a VO_2 film. Unlike the case of gold nanoplates, the quantum trapping of Teflon nanoplates and its release correspond to the insulating and metallic phases of VO_2. Moreover, the switching phenomena can be realized only with a several-nanometers thickness of VO_2.

II. THEORETICAL MODELS

The system in this work is schematically shown in Fig. 1(a), where a gold nanoplate with thickness L_g is suspended in a liquid of bromobenzene. The separation between the nanoplate and the substrate is d. The substrate is composed of a VO_2 film buried under a semi-infinite plate of Teflon. The thicknesses of the top-layer Teflon and VO_2 are denoted as L_T and L_V, respectively. The in-plane dimension of the gold nanoplate is much larger than L_g and d, and it is considered as a slab during our calculations. The Casimir force is calculated by $F_c = -\partial E_c(d)/\partial d$, where $E_c(d)$ is the Casimir energy between the gold nanoplate and the substrate, having the form [23,32]

$$E_c(d) = A\hbar \int_0^\infty \frac{d\xi}{2\pi} \int \frac{d^2\mathbf{k}_\parallel}{(2\pi)^2} \log\det\left[1 - \mathbf{R_1}\cdot\mathbf{R_2} e^{-2k_3 d}\right], \tag{1}$$

where $\hbar$ is the reduced Planck constant, A is the in-plane area, $\mathbf{k}_\parallel$ is the parallel wave vector, $k_3 = \sqrt{k_\parallel^2 + \varepsilon_{\rm liq}(i\xi)\xi^2/c^2}$ is the vertical wave vector, c is the speed of light in vacuum, $\varepsilon_{\rm liq}(i\xi)$ is the permittivity of the intervening liquid evaluated with imaginary frequency $\omega = i\xi$, $\mathbf{R}_{1,2}$ is the 2×2 reflection matrix for layered structures, having the form

$$\mathbf{R_j} = \begin{pmatrix} r_j^s & 0 \\ 0 & r_j^p \end{pmatrix}, \tag{2}$$

where r_j with $j = 1$ and $j = 2$ are the reflection coefficients for the upper and lower layered structures, and the superscripts s and p correspond to the polarizations of transverse electric (**TE**) and transverse magnetic (**TM**) modes, respectively. Note that the temperature T for Eq. (1) equals 0 K and it is an effective approximation as the separation d is smaller than 1 μm for finite temperatures [52]. For a nanoplate suspended in a liquid, the reflection coefficients can be given analytically as follows [19]

$$r^\alpha = \frac{r_{0j}^\alpha + r_{j0}^\alpha e^{-2K_j L_j}}{1 + r_{0j}^\alpha r_{j0}^\alpha e^{-2K_j L_j}}, \tag{3}$$

where $\alpha = s$ and p, L_j is the thickness of the nanoplate, $K_j = \sqrt{k_\parallel^2 + \varepsilon_j(i\xi)\xi^2/c^2}$ is the vertical wave vector, $\varepsilon_j(i\xi)$ is the permittivity of the nanoplate. The subscripts of r_{mn}^α represent the light is incident from the medium m to n (0 means the liquid).

Alternatively, the reflection coefficients for layered structures can be calculated by a transfer matrix method. The general form is given as $r = M_{21}/M_{11}$, where M_{21} and M_{11} are the elements of the M matrix [53]. The M matrix is the multiplications of transmission matrices across different interfaces and propagation matrices in different layers. Considering an arbitrary N-layer system, the M-matrix is given as

$$M = D_{0,1}P(L_1)D_{1,2}P(L_2),\ldots,D_{N-1,N}P(L_N)D_{N,N+1}, \tag{4}$$

where the transmission matrix $D_{j,j+1}$ is given as

$$D_{j,j+1} = \frac{1}{2}\begin{bmatrix} 1+\eta & 1-\eta \\ 1-\eta & 1+\eta \end{bmatrix}, \tag{5}$$

where $\eta = \varepsilon_j(i\xi)K_{j+1}/[\varepsilon_{j+1}(i\xi)K_j]$ for p-polarization and $\eta = K_{j+1}/K_j$ for s-polarization. The propagation matric in the

jth layer (for both s and p polarizations) is written as

$$P_j(L_j) = \begin{bmatrix} e^{K_j L_j} & 0 \\ 0 & e^{-K_j L_j} \end{bmatrix}. \quad (6)$$

For example, we have $N = 2$ for the multilayer substrate in Fig. 1. The M matrix is given by $M = D_{0,1}P(L_1)D_{1,2}P(L_2)D_{2,3}$, where the subscript 0, 1, 2, and 3 represent the media of liquid, Teflon, VO_2, and Teflon (from top to down); the thickness $L_1 = L_T$, $L_2 = L_V$. Note that the forms of transmission matrices given in Eqs. (4) to (6) are valid only for isotropic materials. For anisotropic materials, the separation between TE and TM modes is not applied anymore due to their coupling, and the corresponding transmission matrices are more complicated.

III. RESULTS AND DISCUSSIONS

Figure 1(b) shows the permittivity for different materials, where the used models and parameters are given in the Appendix. The dielectric function of VO_2 changes dramatically under different temperatures. For temperature $T > T_c$, VO_2 is in the metallic phase and it acts as a poor metal. For $T < T_c$, it is in the insulating phase (or called semiconducting phase), and the corresponding dielectric function nearly matches that of intrinsic silicon at low frequency [50]. To create repulsive Casimir forces between two dissimilar plates separated by a liquid, the permittivity should satisfy $\varepsilon_1(i\xi) > \varepsilon_{liq}(i\xi) > \varepsilon_2(i\xi)$ for a vast range of frequency [13]. Clearly, the dielectric functions of gold and VO_2 (either metallic or insulating phase) are larger than that of bromobenzene over a wide range of frequency. Therefore, the Casimir force is always attractive for the layer structure of gold/bromobenzene/VO_2. While the Casimir force for the structure of gold/bromobenzene/Teflon is repulsive instead. Nonetheless, the Casimir equilibria cannot be found for the above two layered structures.

A. Tunable Casimir equilibria for gold nanoplates

Now we consider the Casimir forces as the substrate is composed of a VO_2 film and Teflon [see Fig. 1(a)]. The Casimir pressure ($P_c = F_c/A$) for the thick film of VO_2 is given in Fig. 2(a). The results show that the curves are almost identical for $L_V = 200$, 500, and 1000 nm, indicating the weak impact of the thickness for thick-film configurations. The pressure is repulsive at small separation (e.g., $d < 60$ nm), making the nanoplate stay away from the substrate. As the separation increases further, the Casimir equilibria (zero pressure) occur and quantum traps can be realized for both the metallic (solid lines) and insulating phases (dashed lines). In addition, the equilibrium distance d_c is shifted under the phase transition of VO_2. On the other hand, the thin-film thickness and the phase transition of VO_2 can play an important role in Casimir pressure as shown in Fig. 2(b). For the thickness $L_V = 10$ and 20 nm, quantum traps can be realized for the metallic phase, whereas no-trap is found for the insulating phase. Under such configurations, a switch from quantum trapping of the nanoplate("on" state) to its release ("off" state) can be triggered by the metal-insulator transition of VO_2. However, the quantum trapping occurs for both metallic and insulating phases as the thickness L_V increases to 30 nm, and the "off" state disappears. Compared to the vacuum-separated configuration [51], not only the magnitude of Casimir forces can be modified in a liquid environment, but also the sign could be switched (e.g., from attraction to repulsion for $d = 100$ nm, $L_V = 30$ nm), due to the phase-transition of VO_2.

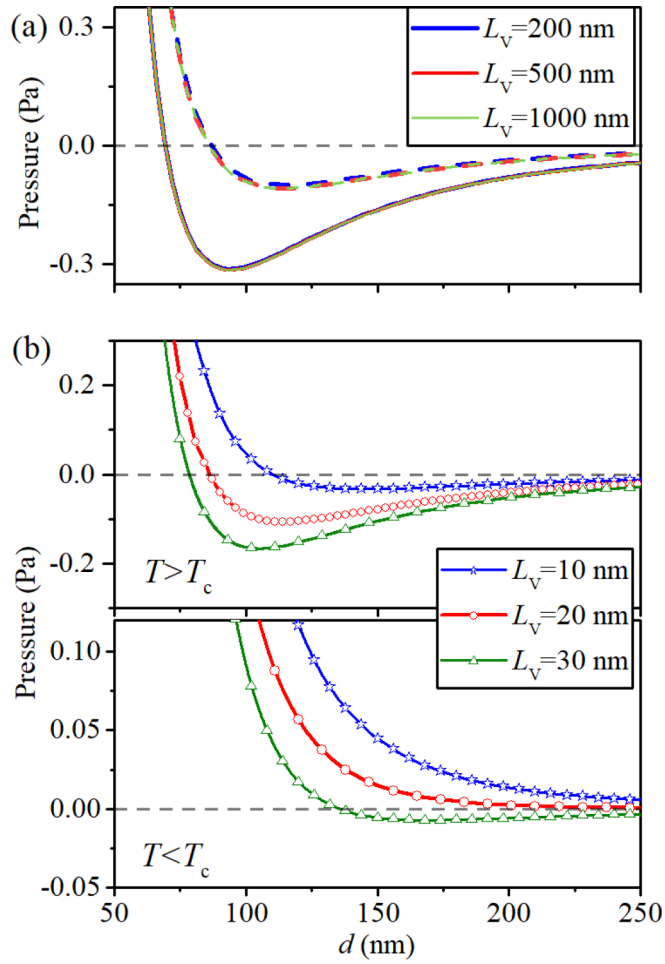

FIG. 2. Casimir pressure via different thicknesses of VO_2, where the thickness $L_T = 45$ nm and $L_g = 40$ nm are fixed. (a) Thick films. The solid and dashed lines represent the pressure for the metallic and insulating phases of VO_2, respectively. (b) Thin films. The positive (negative) sign of the pressure corresponds to the repulsive (attractive) force.

To understand the switch transition from the "on" to the "off" state, the contour plots of Casimir pressure are shown in Fig. 3 under different separations. The sign of pressure is determined by the competition of VO_2 film (attraction) and low-refractive-index Teflon (repulsion). For small separation $d = 30$ nm, the pressure is dominant by the repulsive component as shown in Figs. 3(a) and 3(b). For the metallic phase, the attractive component increases and it compensates the repulsive one as the separation becomes 85 nm ($d \approx d_c$), resulting in Casimir equilibrium [see Fig. 3(c)]. While the repulsion is still dominant for the insulating phase as shown in Fig. 3(d). As d increases further to 150 nm, the Casimir pressure turns out to be dominantly attractive in Fig. 3(e)

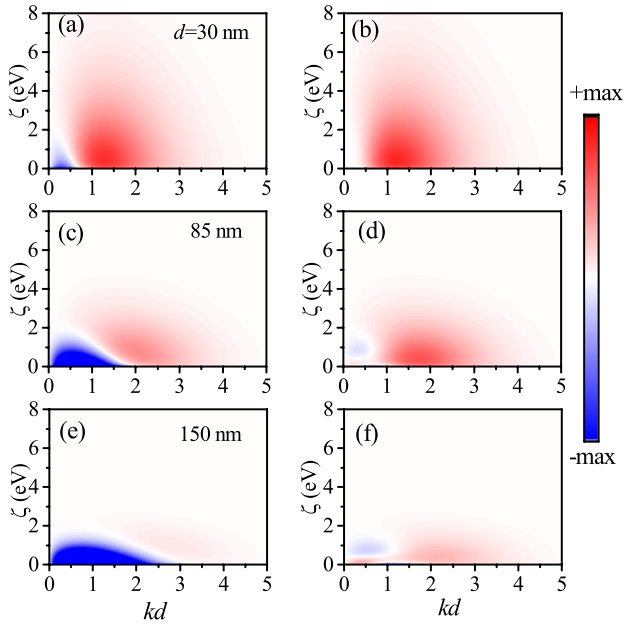

FIG. 3. Casimir pressure contributed from different frequencies and different parallel wave vectors. (a) and (b) $d = 30$ nm; (c) and (d) $d = 85$ nm (close to critical separation); (e) and (f) $d = 150$ nm. (a), (c), and (e) VO_2 in the metallic phase ($T > T_c$); (b), (d), and (f) VO_2 in the insulating phase ($T < T_c$). The layer thicknesses are set as $L_V = 20$ nm and $L_T = 45$ nm.

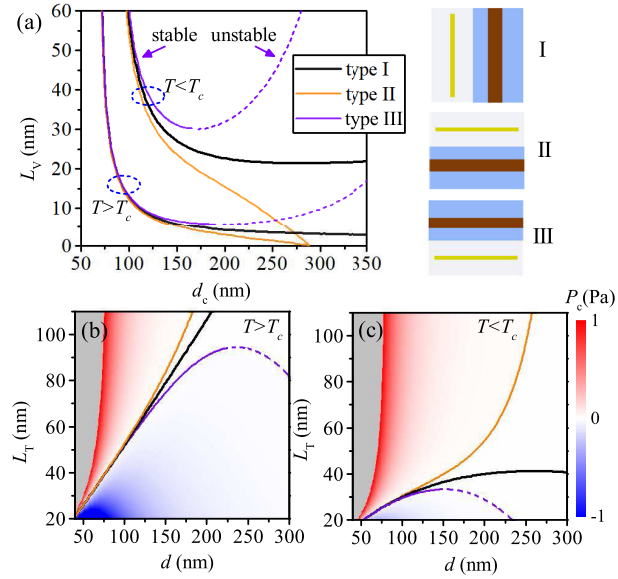

FIG. 4. (a) The equilibrium distances via the thicknesses of VO_2 under three different configurations (see the inset on the right). The thickness L_T is set as 45 nm. The solid (dashed) curves for type III represent stable (unstable) equilibria. Contour plots of Casimir pressure via the thicknesses of coating Teflon for (b) metallic VO_2 and (c) insulating VO_2, where the thickness $L_V = 20$ nm is fixed. In (b) and (c), the gray zones represent a strong repulsive pressure larger than 1 Pa. The colors of the curves denote the same meaning as those in (a).

for the metallic phase, resulting in a restoring force for stable trapping. By contrast, the pressure is still dominant by repulsion for the insulating phase as shown in Fig. 3(f). The pressure maps between the metallic and insulating phases are almost identical for large energy (e.g., > 2 eV), whereas the discrepancy manifests at low energy. The results indicate that the attractive component appears only at low frequency and small k vector for metallic VO_2, where the field cannot penetrate the metal [32]. Conversely, the field can penetrate the thin-film of insulating VO_2 easily, leading to repulsive Casimir forces.

Practically, the influences of gravitation and buoyancy on the force balances should be taken into account. The condition for the force equilibrium is written as $\vec{n} \cdot (\mathbf{F}_c + \mathbf{F}_{GB}) = 0$, where $\vec{n}$ is the unit vector normal to the surface, $F_{GB} = (\rho_g - \rho_{liq}) g L_g A$ is the sum of gravity and buoyancy, g is the gravitational acceleration, $\rho_g \approx 19.3$ g/cm^3 and $\rho_{liq} \approx 1.50$ g/cm^3 is the density of gold and liquid bromobenzene, respectively. The magnitude of F_{GB}/A is about 7.0 mPa as the thickness $L_g = 40$ nm. Three types of configurations are depicted in the inset of Fig. 4(a) for the cross-section views. The type I configuration corresponds to a zero-projection (or weightlessness in aerospace), where the switching from quantum trapping (metallic state) to its release (insulating state) can be obtained as L_V in a proper range, from about 2 to 22 nm. For type II configuration, the attractive F_{GB} can compensate the long-range repulsive Casimir force at large d, leading to stable suspensions for both $T > T_c$ and $T < T_c$. However, the equilibrium distances are different and it can be inferred that the stiffness of trapping for the metallic phase is stronger than that of the insulating phase. For type III configuration (a flipped down system), the switching between trapping and its release can also be realized. Interestingly, there are two equilibrium distances for this configuration. It is not difficult to know that the smaller equilibrium distance (solid lines) is stable, whereas the other one (dashed lines) with larger distance is unstable to small perturbations in position. For both type II and III configurations, the deviations from type I become strong as d_c is large.

In addition to the thickness of VO_2 film, the top-layer Teflon can also play a significant role in the Casimir effect. The plots of Casimir pressure via the thicknesses of the coating Teflon L_T are shown in Figs. 4(b) and 4(c), where $L_V = 20$ nm is fixed. The results show that the switching between quantum trapping and it release occurs only when L_T is larger than about 42 nm (no gravity). The larger the L_T, the larger of the position for Casimir equilibria. As L_T is smaller than 42 nm, the equilibrium distance is also small, and quantum trappings can be realized for both metallic and insulating phases. For comparison, the gravitation and buoyancy are taken into account. Again, strong discrepancies among three configurations occur as the equilibrium positions larger than about 150 nm, resulting from the comparable magnitude of F_{GB} and the Casimir force. The impact of F_{GB} can be further reduced by decreasing the thickness L_g near the skin depth (about 22 nm) [54].

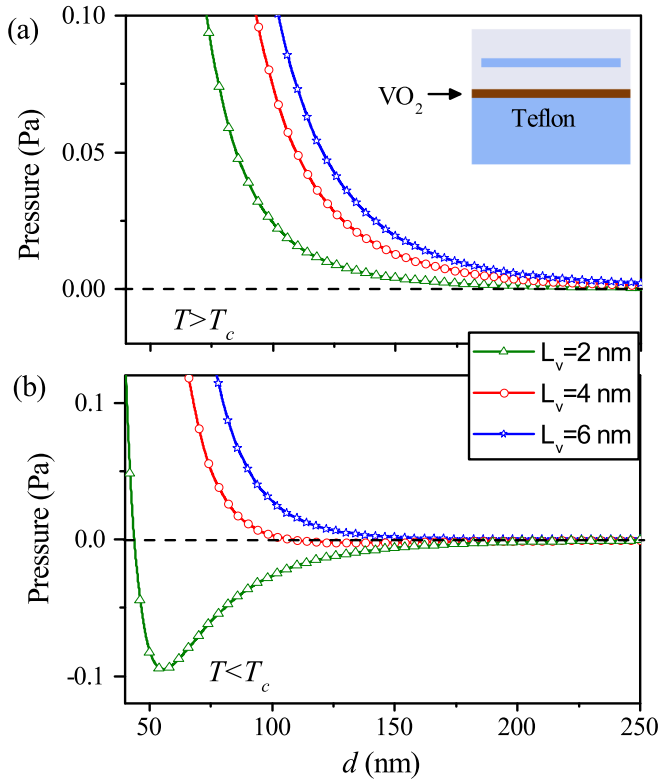

FIG. 5. Casimir pressure for a complementary design. A thin film of VO_2 with thickness L_V is deposited on a Teflon substrate. (a) The metallic VO_2; (b) The insulating VO_2. The thickness of the suspended nanoplate is set as 100 nm.

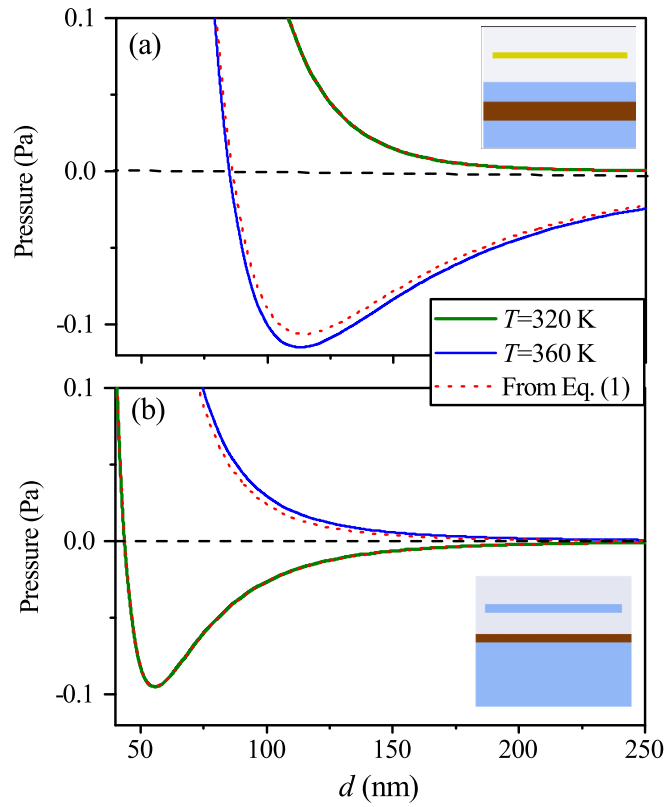

FIG. 6. Casimir pressure calculated for finite temperatures and 0 K approximation from Eq. (1). (a) The trapping and release of a gold nanoplate. The parameters for the substrate are $L_T = 45$ nm and $L_V = 20$ nm. (b) The trapping and release of a Teflon nanoplate. The thickness L_V is set as 2 nm.

B. Tunable Casimir equilibria for Teflon nanoplates

The active control of the low-refractive-index nanoplates can also be significant in many applications. Inspired by the work of the authors of Ref. [32], a complementary design is schematically shown in the inset of Fig. 5(a). A Teflon nanoplate is suspended in a liquid of bromobenzene, and the substrate is a semi-infinite plate of Teflon coated by a VO_2 film (high refractive index). Under such design, the Casimir force is repulsive at very short separation due to the dominant interaction between Teflon/bromobenzene/VO_2. As the separation increases, the attractive interaction from Teflon/bromobenzene/Teflon can be dominant instead, resulting in a stable Casimir trapping. To verify the design, the Casimir pressure is given quantitatively in Figs. 5(a) and 5(b) as a function of separation. Interestingly, the Casimir pressure shows a long-range repulsive behavior for the metallic VO_2, which corresponds to the "off" state. The repulsion pressure becomes stronger as the thickness L_V enlarges from 2 to 6 nm. For $L_V = 2$ nm, a Casimir equilibrium and strong restoring forces can be found when VO_2 is in the insulating phase. Therefore, the quantum trapping and release of a Teflon nanoplate can be achieved under the insulator-to-metal transition of VO_2. As the thickness is 4 nm, the restoring force decreases and the trapping stiffness drops considerably. The calculation results indicate that the Casimir pressure is quite sensitive to the thickness of VO_2. Due to the low density of Teflon (2.1 g/cm^3), the force F_{GB} for the Teflon nanoplate is about 0.6 mPa, which is reduced significantly compared with those of gold nanoplates.

C. Finite temperatures effect

To achieve the phase transition of VO_2, the temperatures of the devices need to be changed. We assume that the dielectric functions of the gold and Teflon are temperature-independent. For organic liquids, the change of refractive index due to the temperature [55] is an order of 10^{-4}/ K, and the permittivity of bromobenzene is also treated as temperature-independent. Nonetheless, it is interesting to check the finite temperature effect on Casimir forces. The integral over frequency ξ in Eq. (1) now is replaced by a discrete summation [56]

$$\frac{\hbar}{2\pi}\int_0^\infty d\xi \leftrightarrow k_b T \sum_{n=0}^{\infty\,\prime}, \tag{7}$$

where ξ is replaced by discrete Matsubara frequencies $\xi_n = 2\pi\frac{k_b T}{\hbar}n (n = 0, 1, 2, 3\ldots)$, k_B is the Boltzmann's constant and the prime denotes a prefactor 1/2 for the term $n = 0$. The Casimir pressures under different temperatures are shown in Figs. 6(a) and 6(b), where two different designs are demonstrated. It is found that the curves for temperature 320 K (insulating phase) overlap with those calculated from Eq. (1). For the temperature of 360 K, there is only a small deviation between 0 and 360 K. Overall, the calculation

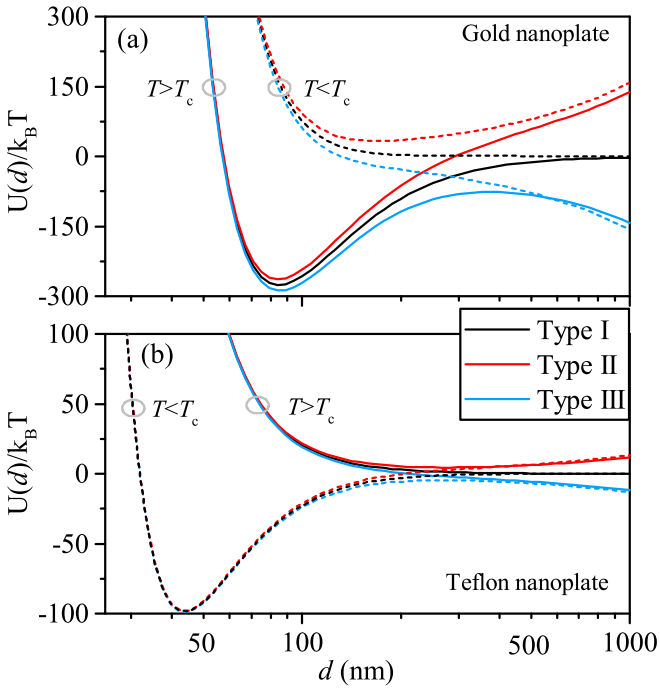

FIG. 7. The total energy of (a) a suspended gold nanoplate and (b) a Teflon nanoplate under different types of gravity projection. The solid and dashed lines represent the cases for the metallic VO_2(T = 360 K) and insulating VO_2(T = 320 K), respectively. The in-plane area A is set as 10 μm × 10 μm. Other parameters are kept the same as those in Fig. 6.

results from 320 and 360 K confirm the accuracy of the 0 K approximation. Recently, the switching between repulsive and attractive Casimir forces based on PCM has also been reported [57], where the equilibrium distances for switching occur only at several nanometers. The equilibrium distances in our work are more accessible to experiments, and it can be tuned by designing the geometric thickness of VO_2 and the Teflon.

D. Effect of Brownian motion

In a real configuration, the position of a nanoplate has a fluctuation around the equilibrium distance due to the Brownian motion. To evaluate the effect, the total energy of the suspended nanoplate should be known, which are written as $U(d) = E_c + \Lambda \times (E_g + E_b)$, where E_c is the Casimir energy given by Eq. (1), $E_g = \rho_g g L_g A d$ and $E_b = -\rho_{\rm liq} g L_g A d$ are, respectively, the energies generated from the gravity and buoyancy [58]. The coefficient Λ is the parameter depending on the gravity projection. For type I configuration (see the inset of Fig. 4), $\Lambda = 0$. While $\Lambda = 1$ and -1 for type II and type III configurations. The total energy of a gold and Teflon nanoplate are shown in Figs. 7(a) and 7(b), where the in-plane area $A = 10\ \mu\text{m} \times 10\ \mu\text{m}$. The minimum of $U(d)/k_BT$ corresponds to the equilibrium distance d_c. Clearly, stable quantum trapping can be realized for a gold (Teflon) nanoplate when VO_2 is in the metallic (insulating) phase. Due to the balance of repulsive Casimir force and gravity, stable trapping can also be realized for type II configuration. According to the work of the authors of Refs. [58,59], the transition rate due to the Brownian motion is proportional to $\exp(-\triangle U/k_BT)$. It is easy to infer that the possibility from Casimir equilibria to stiction is negligible since $\triangle U/k_BT$ is very larger (e.g., over 10^4). For a flipped down system (type III), however, there is a possibility that the nanoplate can escape from the quantum trapping to the free-liquid regime($d \to \infty$). Fortunately, the energy barrier $\triangle U/k_BT$ for such transition is the order of 10^2 as shown in Figs. 7(a) and 7(b), and the rate of the escape is also negligible.

IV. CONCLUSION

In summary, the Casimir forces between a nanoplate and a layered structure containing VO_2 films are investigated. In a liquid-separated environment, not only the magnitude of Casimir forces can be modified, but also the sign could be switched (e.g., from attraction to repulsion) due to the phase-transition of VO_2. Moreover, a stable Casimir suspension of nanoplates and its tunability are revealed. For a gold nanoplate, a switch from the quantum trapping to its release is obtained under the metal-to-insulator transition of VO_2. In addition, the quantum trapping and release of a Teflon nanoplate are demonstrated with a complementary design. The switching performances due to the layer thicknesses, gravitation, and temperatures are discussed as well. Theoretically, the bromobenzene can be substituted by other high-refractive-index liquids (e.g., glycerol and styrene [14]) as long as the boiling points are larger than T_c. The Teflon can also be replaced by other low-refractive-index materials (e.g., mesoporous silica [16]). This work offers the possibility of designing switchable devices in MEMS/NEMS, resulting from the quantum fluctuations of the electromagnetic field.

ACKNOWLEDGMENTS

This work is supported by the National Natural Science Foundation of China (Grants No. 11804288, No. 11704254, No. 61571386, and No. 61974127), and the Innovation Scientists and Technicians Troop Construction Projects of Henan Province. The research of L.X.G. is further supported by Nanhu Scholars Program for Young Scholars of XYNU.

APPENDIX A: PERMITTIVITY OF GOLD

Here a generalized Drude-Lorentz model is applied for the permittivity of gold [60]

$$\varepsilon(i\xi) = \varepsilon_D(i\xi) + \varepsilon_L(i\xi), \tag{A1}$$

where the Drude term is given by

$$\varepsilon_D(i\xi) = \varepsilon_\infty + \frac{\gamma\sigma}{\xi(\xi+\gamma)}, \tag{A2}$$

TABLE I. The fitted parameters for Lorentz poles of gold [60].

jth	σ_j	Ω_j
1	$-0.01743 + 0.3059I$	$2.6905 - 0.16645I$
2	$1.0349 + 1.2919I$	$2.8772 - 0.44473I$
3	$1.2274 + 2.5605I$	$3.7911 - 0.81981I$
4	$9.85 + 37.614I$	$4.8532 - 13.891I$

TABLE II. The parameters for the metallic and insulating VO_2 [50].

jth	$S_j(T > T_c)$	$\omega_j(T > T_c)$	$\Gamma_j(T > T_c)$
1	1.816	0.86	0.95
2	0.972	2.8	0.23
3	1.04	3.48	0.28
4	1.05	4.6	0.34
jth	$S_j(T < T_c)$	$\omega_j(T < T_c)$	$\Gamma_j(T < T_c)$
1	0.79	1.02	0.55
2	0.474	1.30	0.55
3	0.483	1.50	0.50
4	0.536	2.75	0.22
5	1.316	3.49	0.47
6	1.060	3.76	0.38
7	0.99	5.1	0.385

where $\varepsilon_\infty = 0.83409$, $\sigma = 3134.5$ eV, and $\gamma = 0.02334$ eV. The Lorentz term is described by four pairs of poles:

$$\varepsilon_L(i\xi) = \sum_{j=1}^{4}\left(\frac{i\sigma_j}{i\xi - \Omega_j} + \frac{i\sigma_j^*}{i\xi + \Omega_j^*}\right), \tag{A3}$$

where σ_j and Ω_j are the generalized conductivity and resonant frequency of the jth Lorentz pole. The star superscripts represent the operation of complex conjugation. The generalized Drude-Lorentz model respects causality, and it can represent the exact physical resonances in the material. The parameters for the model are listed in Table I.

APPENDIX B: PERMITTIVITY OF VO_2

For temperature $T > T_c$, VO_2 is in the metallic phase, and the permittivity is given by [50,51]

$$\varepsilon(i\xi) = 1 + \frac{\omega_p^2}{\xi(\xi+\gamma)} + \frac{\varepsilon_\infty - 1}{1 + \xi^2/\omega_\infty^2} + \sum_{j=1}^{4}\frac{s_j}{1 + (\xi/\omega_j)^2 + \Gamma_j\xi/\omega_j}, \tag{B1}$$

TABLE III. The parameters for Teflon (left) and bromobenzene (right) [14].

jth	C_j	ω_j(eV)	C_j	ω_j(eV)
1	0.00930	0.0003	0.0544	0.00502
2	0.0183	0.0076	0.0184	0.0309
3	0.139	0.0557	0.0475	0.111
4	0.112	0.126	0.532	6.75
5	0.195	6.71	0.645	13.3
6	0.438	18.6	0.240	24.0
7	0.106	42.1	0.00927	99.9
8	0.0386	77.6		

where $\varepsilon_\infty = 3.95$, $\omega_p = 3.33$ eV, and $\gamma = 0.66$ eV. The parameters s_j and Γ_j represent, respectively, the strength and linewidth of the jth oscillator (resonant frequency ω_j).

For temperature $T < T_c$, VO_2 is in the insulating phase, and the permittivity is described as

$$\varepsilon(i\xi) = 1 + \frac{\varepsilon_\infty - 1}{1 + \xi^2/\omega_\infty^2} + \sum_{j=1}^{7}\frac{s_j}{1 + (\xi/\omega_j)^2 + \Gamma_j\xi/\omega_j}, \tag{B2}$$

where $\varepsilon_\infty = 4.26$ and $\omega_\infty = 15$ eV. The above equations for metallic and insulating VO_2 are valid for a wide range of frequency (up to about 10 eV), which is a modification version of Ref. [61]. The parameters are listed in Table II.

APPENDIX C: PERMITTIVITY OF TEFLON AND BROMOBENZENE

The permittivity for the Teflon and bromobenzene are given by the oscillator model [14]

$$\varepsilon(i\xi) = 1 + \sum_{j}^{n}\frac{C_j}{1 + (\xi/\omega_j)^2}, \tag{C1}$$

where C_j corresponds to the oscillator strength for the jth resonance, and ω_j is the corresponding resonant frequency. The values of C_j and ω_j listed in Table III are fitted from the experimental data in a wide range of frequency.

[1] S. E. Lyshevski, *MEMS and NEMS: Systems, Devices, and Structures* (CRC Press, Boca Raton, FL, 2018).
[2] H. G. Craighead, Science **290**, 1532 (2000).
[3] K. Eom, H. S. Park, D. S. Yoon, and T. Kwon, Phys. Rep. **503**, 115 (2011).
[4] R. Xu, S. Zhou, and W. J. Li, IEEE Sens. J. **12**, 1166 (2011).
[5] J. Wang, *Nanomachines: Fundamentals and Applications* (John Wiley & Sons, New York, 2013).
[6] E. Buks and M. L. Roukes, Phys. Rev. B **63**, 033402 (2001).
[7] H. Chan, V. Aksyuk, R. Kleiman, D. Bishop, and F. Capasso, Science **291**, 1941 (2001).
[8] H. B. G. Casimir, Proc. Kon. Ned. Akad. Wet. **51**, 793 (1948).
[9] G. L. Klimchitskaya, U. Mohideen, and V. M. Mostepanenko, Rev. Mod. Phys. **81**, 1827 (2009).
[10] V. A. Yampol'skii, S. Savel'ev, Z. A. Mayselis, S. S. Apostolov, and F. Nori, Phys. Rev. Lett. **101**, 096803 (2008).
[11] V. A. Yampol'skii, S. Savel'ev, Z. A. Maizelis, S. S. Apostolov, and F. Nori, Phys. Rev. A **82**, 032511 (2010).
[12] L. M. Woods, D. A. R. Dalvit, A. Tkatchenko, P. Rodriguez-Lopez, A. W. Rodriguez, and R. Podgornik, Rev. Mod. Phys. **88**, 045003 (2016).
[13] J. N. Munday, F. Capasso, and V. A. Parsegian, Nature **457**, 170 (2009).
[14] P. J. van Zwol and G. Palasantzas, Phys. Rev. A **81**, 062502 (2010).
[15] A. D. Phan and N. A. Viet, Phys. Rev. A **84**, 062503 (2011).
[16] M. Dou, F. Lou, M. Boström, I. Brevik, and C. Persson, Phys. Rev. B **89**, 201407(R) (2014).

[17] F. S. S. Rosa, D. A. R. Dalvit, and P. W. Milonni, Phys. Rev. Lett. **100**, 183602 (2008).

[18] R. Zhao, J. Zhou, T. Koschny, E. N. Economou, and C. M. Soukoulis, Phys. Rev. Lett. **103**, 103602 (2009).

[19] R. Zhao, T. Koschny, E. N. Economou, and C. M. Soukoulis, Phys. Rev. B **83**, 075108 (2011).

[20] G. Song, R. Zeng, M. Al-Amri, J. Xu, C. Zhu, P. He, and Y. Yang, Opt. Express **26**, 34461 (2018).

[21] A. G. Grushin and A. Cortijo, Phys. Rev. Lett. **106**, 020403 (2011).

[22] L. Chen and S. Wan, Phys. Rev. B **85**, 115102 (2012).

[23] W. Nie, R. Zeng, Y. Lan, and S. Zhu, Phys. Rev. B **88**, 085421 (2013).

[24] P. Rodriguez-Lopez, W. J. M. Kort-Kamp, D. A. R. Dalvit, and L. M. Woods, Nat. Commun. **8**, 14699 (2017).

[25] W.-K. Tse and A. H. MacDonald, Phys. Rev. Lett. **109**, 236806 (2012).

[26] N. Khusnutdinov and L. M. Woods, JETP Lett. **110**, 183 (2019).

[27] L. Tang, M. Wang, C. Y. Ng, M. Nikolic, C. T. Chan, A. W. Rodriguez, and H. B. Chan, Nat. Photon. **11**, 97 (2017).

[28] M. Levin, A. P. McCauley, A. W. Rodriguez, M. T. Homer Reid, and S. G. Johnson, Phys. Rev. Lett. **105**, 090403 (2010).

[29] A. W. Rodriguez, J. N. Munday, J. D. Joannopoulos, F. Capasso, D. A. R. Dalvit, and S. G. Johnson, Phys. Rev. Lett. **101**, 190404 (2008).

[30] S. J. Rahi and S. Zaheer, Phys. Rev. Lett. **104**, 070405 (2010).

[31] A. W. Rodriguez, A. P. McCauley, D. Woolf, F. Capasso, J. D. Joannopoulos, and S. G. Johnson, Phys. Rev. Lett. **104**, 160402 (2010).

[32] R. Zhao, L. Li, S. Yang, W. Bao, Y. Xia, P. Ashby, Y. Wang, and X. Zhang, Science **364**, 984 (2019).

[33] G. Torricelli, P. J. Van Zwol, O. Shpak, G. Palasantzas, V. B. Svetovoy, C. Binns, B. J. Kooi, P. Jost, and M. Wuttig, Adv. Funct. Mater. **22**, 3729 (2012).

[34] M. Sedighi, W. H. Broer, G. Palasantzas, and B. J. Kooi, Phys. Rev. B **88**, 165423 (2013).

[35] G. Torricelli, P. J. van Zwol, O. Shpak, C. Binns, G. Palasantzas, B. J. Kooi, V. B. Svetovoy, and M. Wuttig, Phys. Rev. A **82**, 010101(R) (2010).

[36] C. Abbas, B. Guizal, and M. Antezza, Phys. Rev. Lett. **118**, 126101 (2017).

[37] A. D. Phan, N. A. Viet, N. A. Poklonski, L. M. Woods, and C. H. Le, Phys. Rev. B **86**, 155419 (2012).

[38] N. Khusnutdinov, R. Kashapov, and L. M. Woods, 2D Mater. **5**, 035032 (2018).

[39] Z. Shao, X. Cao, H. Luo, and P. Jin, NPG Asia Mater. **10**, 581 (2018).

[40] A. M. N. F. Zylbersztejn and N. F. Mott, Phys. Rev. B **11**, 4383 (1975).

[41] S.-H. Wu, M. Chen, M. T. Barako, V. Jankovic, P. W. C. Hon, L. A. Sweatlock, and M. L. Povinelli, Optica **4**, 1390 (2017).

[42] H. Liu, J. Lu, and X. R. Wang, Nanotechnology **29**, 024002 (2017).

[43] M. A. Kats, D. Sharma, J. Lin, P. Genevet, R. Blanchard, Z. Yang, M. M. Qazilbash, D. Basov, S. Ramanathan, and F. Capasso, Appl. Phys. Lett. **101**, 221101 (2012).

[44] P. J. van Zwol, L. Ranno, and J. Chevrier, Phys. Rev. Lett. **108**, 234301 (2012).

[45] A. Cavalleri, C. Tóth, C. W. Siders, J. A. Squier, F. Ráksi, P. Forget, and J. C. Kieffer, Phys. Rev. Lett. **87**, 237401 (2001).

[46] M. Rini *et al.*, Appl. Phys. Lett. **92**, 181904 (2008).

[47] M. M. Qazilbash, Z. Q. Li, V. Podzorov, M. Brehm, F. Keilmann, B. G. Chae, H.-T. Kim, and D. N. Basov, Appl. Phys. Lett. **92**, 241906 (2008).

[48] M. Nakano, K. Shibuya, D. Okuyama, T. Hatano, S. Ono, M. Kawasaki, Y. Iwasa, and Y. Tokura, Nature **487**, 459 (2012).

[49] E. G. Galkina, B. A. Ivanov, S. Savel'ev, V. A. Yampol'skii, and F. Nori, Phys. Rev. B **80**, 125119 (2009).

[50] I. Pirozhenko and A. Lambrecht, Phys. Rev. A **77**, 013811 (2008).

[51] R. Castillo-Garza, C.-C. Chang, D. Jimenez, G. L. Klimchitskaya, V. M. Mostepanenko, and U. Mohideen, Phys. Rev. A **75**, 062114 (2007).

[52] K. A. Milton, J. Phys. A **37**, R209 (2004).

[53] T. Zhan, X. Shi, Y. Dai, X. Liu, and J. Zi, J. Phys.: Condens. Matter **25**, 215301 (2013).

[54] M. Lisanti, D. Iannuzzi, and F. Capasso, Proc. Natl. Acad. Sci. USA **102**, 11989 (2005).

[55] W. Li, P. N. Segre, R. Gammon, J. V. Sengers, and M. Lamvik, J. Chem. Phys. **101**, 5058 (1994).

[56] S. J. Rahi, T. Emig, N. Graham, R. L. Jaffe, and M. Kardar, Phys. Rev. D **80**, 085021 (2009).

[57] M. Boström, M. Dou, O. I. Malyi, P. Parashar, D. F. Parsons, I. Brevik, and C. Persson, Phys. Rev. B **97**, 125421 (2018).

[58] A. D. Phan, L. M. Woods, D. Drosdoff, I. V. Bondarev, and N. A. Viet, Appl. Phys. Lett. **101**, 113118 (2012).

[59] A. W. Rodriguez, D. Woolf, A. P. McCauley, F. Capasso, J. D. Joannopoulos, and S. G. Johnson, Phys. Rev. Lett. **105**, 060401 (2010).

[60] H. S. Sehmi, W. Langbein, and E. A. Muljarov, Phys. Rev. B **95**, 115444 (2017).

[61] H. W. Verleur, A. S. Barker, Jr., and C. N. Berglund, Phys. Rev. **172**, 788 (1968).